Computational analysis of thin film InGaAs/GaAs quantum well solar cells with back side light trapping structures

Claiborne O. McPheeters[1] and Edward T. Yu[1,*]

[1]*Microelectronics Research Center, Department of Electrical and Computer Engineering, University of Texas, Austin, 10100 Burnet Rd, Bldg 160, Austin, TX 78758, USA*
[*]*ety@ece.utexas.edu*

Abstract: Simulations of thin film (~2.5 µm thick) InGaAs/GaAs quantum well solar cells with various back side reflective and planar, symmetric scattering structures used for light trapping have been performed using rigorous coupled-wave analysis. Two-dimensional periodic metal/dielectric scattering structures were numerically optimized for Airmass 0 photocurrent generation for each device structure. The simulation results indicate that the absorption spectra of devices with both reflective and scattering structures are largely determined by the Fabry-Perot resonance characteristics of the thin film device structure. The scattering structures substantially increase absorption in the quantum wells at wavelengths longer than the GaAs absorption edge through a combination of coupling to modes of the thin film device structures and by reducing parasitic metal absorption compared to planar metal reflectors. For Airmass 0 illumination and 100% carrier collection, the estimated short-circuit current density of devices with $In_{0.3}Ga_{0.7}As$/GaAs quantum wells improves by up to 4.6 mA/cm^2 (15%) relative to a GaAs homojunction device, with the improvement resulting approximately equally from scattering of light into thin film modes and reduction of metal absorption compared to a planar reflective layer.

OCIS codes: (040.5350) Photovoltaic; (230.5590) Quantum-well, -wire and -dot devices; (050.6624) Subwavelength structures; (250.0250) Optoelectronics; (350.6050) Solar energy.

References and links

1. W. Shockley and H. J. Queisser, "Detailed balance limit of efficiency of p-n junctions solar cells," J. Appl. Phys. **32**(3), 510–519 (1961).
2. M. Mazzer, K. W. J. Barnham, I. M. Ballard, A. Bessiere, A. Ioannides, D. C. Johnson, M. C. Lynch, T. N. D. Tibbits, J. S. Roberts, G. Hill, and C. Calder, "Progress in quantum well solar cells," Thin Solid Films **511–512**, 76–83 (2006).
3. J. G. J. Adams, B. C. Browne, I. M. Ballard, J. P. Connolly, N. L. A. Chan, A. Ioannides, W. Elder, P. N. Stavrinou, K. W. J. Barnham, and N. J. Ekins-Daukes, "Recent results for single-junction and tandem quantum well solar cells," Prog. Photovolt. Res. Appl. **19**(7), 865–877 (2011).
4. R. M. Farrell, C. J. Neufeld, S. C. Cruz, J. R. Lang, M. Iza, S. Keller, S. Nakamura, S. P. DenBaars, U. K. Mishra, and J. S. Speck, "High quantum efficiency InGaN/GaN multiple quantum well solar cells with spectral response extending out to 520 nm," Appl. Phys. Lett. **98**(20), 201107 (2011).
5. A. Freundlich, A. Fotkatzikis, L. Bhusal, L. Williams, A. Alemu, W. Zhu, J. A. H. Coaquira, A. Feltrin, and G. Radhakrishnan, "III–V dilute nitride-based multi-quantum well solar cell," J. Cryst. Growth **301–302**, 993–996 (2007).
6. R. B. Laghumavarapu, M. El-Emawy, N. Nuntawong, A. Moscho, L. F. Lester, and D. L. Huffaker, "Improved device performance of InAs/GaAs quantum dot solar cells with GaP strain compensation layers," Appl. Phys. Lett. **91**(24), 243115 (2007).
7. S. M. Hubbard, C. D. Cress, C. G. Bailey, R. P. Raffaelle, S. G. Bailey, and D. M. Wilt, "Effect of strain compensation on quantum dot enhanced GaAs solar cells," Appl. Phys. Lett. **92**(12), 123512 (2008).
8. C. G. Bailey, D. V. Forbes, R. P. Raffaelle, and S. M. Hubbard, "Near 1 V open circuit voltage InAs/GaAs quantum dot solar cells," Appl. Phys. Lett. **98**(16), 163105 (2011).

9. V. Popescu, G. Bester, M. C. Hanna, A. G. Norman, and A. Zunger, "Theoretical and experimental examination of the intermediate-band concept for strain-balanced (In,Ga)As/Ga(As,P) quantum dot solar cells," Phys. Rev. B **78**(20), 205321 (2008).

10. W. U. Huynh, J. J. Dittmer, and A. P. Alivisatos, "Hybrid nanorod-polymer solar cells," Science **295**(5564), 2425–2427 (2002).

11. M. Law, L. E. Greene, J. C. Johnson, R. Saykally, and P. Yang, "Nanowire dye-sensitized solar cells," Nat. Mater. **4**(6), 455–459 (2005).

12. L. Tsakalakos, J. Balch, J. Fronheiser, B. A. Korevaar, O. Sulima, and J. Rand, "Silicon nanowire solar cells," Appl. Phys. Lett. **91**(23), 233117 (2007).

13. J. Kupec, R. L. Stoop, and B. Witzigmann, "Light absorption and emission in nanowire array solar cells," Opt. Express **18**(26), 27589–27605 (2010).

14. G. Wei, K.-T. Shiu, N. C. Giebink, and S. R. Forrest, "Thermodynamic limits of quantum photovoltaic cell efficiency," Appl. Phys. Lett. **91**(22), 223507 (2007).

15. S. P. Bremner, R. Corkish, and C. B. Honsberg, "Detailed balance efficiency limits with quasi-Fermi level variations," IEEE Trans. Electron. Dev. **46**(10), 1932–1939 (1999).

16. A. Luque and A. Martí, "Increasing the efficiency of ideal solar cells by photon induced transitions at intermediate levels," Phys. Rev. Lett. **78**(26), 5014–5017 (1997).

17. M. Zeman and J. Krc, "Nano-structures for light management in optoelectronic devices," Proc. 6th Intl. Conf. on Adv. Semicond. Devices and Microsystems, Smolenice, Slovakia, pp. 299–302 (2006).

18. C. Rockstuhl and F. Lederer, "Photon management by metallic nanodiscs in thin film solar cells," Appl. Phys. Lett. **94**(21), 213102 (2009).

19. P. Spinelli, V. E. Ferry, J. van de Groep, M. van Lare, M. A. Verschuuren, R. E. I. Schropp, H. A. Atwater, and A. Polman, "Plasmonic light trapping in thin-film Si solar cells," J. Opt. **14**(2), 024002 (2012).

20. E. T. Yu and J. van de Lagemaat, "Photon management for photovoltaics," MRS Bull. **36**(06), 424–428 (2011).

21. I. Serdiukova, C. Monier, M. F. Vilela, and A. Freundlich, "Critical built-in electric field for an optimum carrier collection in multiquantum well *p-i-n* diodes," Appl. Phys. Lett. **74**(19), 2812–2814 (1999).

22. A. Alemu, J. A. H. Coaquira, and A. Freundlich, "Dependence of device performance on carrier escape sequence in multi-quantum-well *p-i-n* solar cells," J. Appl. Phys. **99**(8), 084506 (2006).

23. E. Yablonovitch, T. Gmitter, J. P. Harbison, and R. Bhat, "Extreme selectivity in the lift-off of epitaxial GaAs films," Appl. Phys. Lett. **51**(26), 2222–2224 (1987).

24. J. J. Schermer, P. Mulder, G. J. Bauhuis, M. M. A. J. Voncken, J. van Deelen, E. Haverkamp, and P. K. Larsen, "Epitaxial lift-off for large area thin film III/V devices," Phys. Status Solidi **202**(4), 501–508 (2005) (a).

25. D. Shahrjerdi, S. W. Bedell, C. Ebert, C. Bayram, B. Hekmatshoar, K. Fogel, P. Lauro, M. Gaynes, T. Gokmen, J. A. Ott, and D. K. Sadana, "High-efficiency thin-film InGaP/InGaAs/Ge tandem solar cells enabled by controlled spalling technology," Appl. Phys. Lett. **100**(5), 053901 (2012).

26. C. O. McPheeters, D. Hu, D. M. Schaadt, and E. T. Yu, "Semiconductor heterostructures and optimization of light-trapping structures for efficient thin-film solar cells," J. Opt. **14**(2), 024007 (2012).

27. G. Bastard, *Wave Mechanics Applied to Semiconductor Heterostructures* (Wiley, 1991), Chap. 7.

28. M. Fox, *Optical Properties of Solids* (Oxford University Press, 2001), Chap. 1.

29. RSoft Design Group, *DiffractMOD User Guide (v. 3.2)*, (2011) p. 39.

30. D. E. Goldberg, *Genetic Algorithms in Search, Optimization, and Machine Learning* (Addison-Wesley, 1989).

31. C. O. McPheeters, C. J. Hill, S. H. Lim, D. Derkacs, D. Z. Ting, and E. T. Yu, "Improved performance of In(Ga)As/GaAs quantum dot solar cells via light scattering by nanoparticles," J. Appl. Phys. **106**(5), 056101 (2009).

32. C. J. Hwang, "Optical properties of *n*-type GaAs. I. Determination of hole diffusion length from optical absorption and photoluminescence measurements," J. Appl. Phys. **40**(9), 3731–3739 (1969).

33. E. Vigil and P. Diaz, "Concentration dependence of the electron diffusion length in *p*-type GaAs," Cryst. Res. Technol. **19**(2), 285–290 (1984).

34. H. C. Casey, Jr., B. I. Miller, and E. Pinkas, "Variation of minority-carrier diffusion length with carrier concentration in GaAs liquid-phase epitaxial layers," J. Appl. Phys. **44**(3), 1281–1287 (1973).

35. G. J. Bauhuis, P. Mulder, J. J. Schermer, E. J. Haverkamp, J. van Deelen, and P. K. Larsen, "High efficiency thin film GaAs solar cells with improved radiation hardness," Proc. 20th European Photovolt. Solar Energy Conf., pp. 468–471 (2005).

36. G. J. Bauhuis, P. Mulder, E. J. Haverkamp, J. C. C. M. Huijben, and J. J. Schermer, "26.1% thin-film GaAs solar cell using epitaxial lift-off," Sol. Energy Mater. Sol. Cells **93**(9), 1488–1491 (2009).

37. T. K. Gaylord and M. G. Moharam, "Analysis and applications of optical diffraction by gratings," Proc. IEEE **73**(5), 894–937 (1985).

38. S. Adachi, "Model dielectric constants of GaP, GaAs, GaSb, InP, InAs, and InSb," Phys. Rev. B Condens. Matter **35**(14), 7454–7463 (1987).

39. E. D. Palik, *Handbook of Optical Constants of Solids* (Academic Press, 1998).

40. B. J. Soller and D. G. Hall, "Energy transfer at optical frequencies to silicon-based waveguiding structures," J. Opt. Soc. Am. A **18**(10), 2577–2584 (2001).

41. D. Derkacs, W. V. Chen, P. M. Matheu, S. H. Lim, P. K. L. Yu, and E. T. Yu, "Nanoparticle-induced light scattering for improved performance of quantum-well solar cells," Appl. Phys. Lett. **93**(9), 091107 (2008).

42. J. Zou, D. J. H. Cockayne, and B. F. Usher, "Misfit dislocations and critical thickness in InGaAs/GaAs heterostructure systems," J. Appl. Phys. **73**(2), 619–626 (1993).
43. Y. C. Chen, P. K. Bhattacharya, and J. Singh, "Accurate determination of misfit strain, layer thickness, and critical layer thickness in ultrathin buried strained InGaAs/GaAs layer by x-ray diffraction," J. Vac. Sci. Technol. B **10**(2), 769–771 (1992).
44. Z. Yu, A. Raman, and S. Fan, "Fundamental limit of light trapping in grating structures," Opt. Express **18**(S3 Suppl 3), A366–A380 (2010).
45. E. F. Schubert, *Light-Emitting Diodes* (Cambridge University Press, 2006) p.206.
46. A. K. Saxena, "The conduction band structure and deep levels in Ga$_{1-x}$Al$_x$As alloys from a high-pressure experiment," J. Phys. Chem. **13**, 4323–4334 (1980).
47. E. Yablonovitch, "Statistical ray optics," J. Opt. Soc. Am. **72**(7), 899–907 (1982).
48. Z. Yu, A. Raman, and S. Fan, "Fundamental limit of nanophotonic light trapping in solar cells," Proc. Natl. Acad. Sci. U.S.A. **107**(41), 17491–17496 (2010).
49. A. Luque, A. Martí, and A. J. Nozik, "Solar cells based on quantum dots: multiple exciton generation and intermediate bands," MRS Bull. **32**(03), 236–241 (2007).

1. Introduction

Photovoltaic devices incorporating quantum confined semiconductors are a subject of considerable interest, which in part results from theoretical studies indicating that such devices can achieve power conversion efficiencies considerably higher than the Shockley-Queisser limit of ~31% for homojunction solar cells [1]. Solar cells that consist of or contain epitaxially grown semiconductor heterostructures or nanostructures, such as quantum wells (QWs) [2–5], quantum dots [6–9], and nanowires [10–13], have been proposed for realizing such device concepts. However, experimental results to-date for such devices [2–12] demonstrate practical performance far below their theoretical limits [14–16] and below the Shockley-Queisser limit.

Simultaneously, there is great interest in developing novel structures for light trapping in solar cells, and in improving existing approaches for light trapping. "Light trapping" refers generally to approaches for improving absorption efficiency in solar cells by increasing the effective path length of photons in device structures [17–20]. Periodic structures are appealing for understanding light trapping because of the relative ease with which they can be analyzed and optimized using rigorous electromagnetic simulations with appropriate boundary conditions. Planar, symmetric structures that can be realized lithographically have added appeal from the perspective of device fabrication, as numerous techniques exist for creating periodic structures with micrometer and sub-micrometer feature sizes.

This work presents the results of electromagnetic simulations of thin film III-V quantum well solar cells (QWSCs) with planar, symmetric light trapping structures that have been optimized for Airmass (AM) 0 photocurrent generation. Device structures with intrinsic regions of ~100-300 nm, such as those investigated here, facilitate a sufficiently large electric field in the junction to collect carriers photogenerated in QW sub-band states with high probability, based on the results of Refs. [21] and [22]. The AM 0 spectrum has been used here because high efficiency thin film devices, like the QWSCs in this work, may be appealing in space power applications for their potential to achieve large mass-specific power [W/kg] and the possibility to manufacture them relatively inexpensively using thin film exfoliation techniques that enable substrate re-use to reduce cost [23–25]. However, the observations and conclusions drawn in this study are also expected to apply in situations for which other illumination spectra are relevant, such as AM 1.5 for terrestrial solar applications, e.g. concentrating photovoltaic systems.

2. Computational approach

Rigorous coupled-wave analysis (RCWA) electromagnetic simulations of thin film solar cells containing III-V semiconductor QWs have been performed to investigate how the device structure, in combination with that of periodic light trapping structures, affects photocurrent generation. Polarization-dependent absorption in the QWs, which results from strain splitting of the heavy- and light-hole valence bands, has been modeled using calculations based on a

four band Kane model [26]. Due to the fact that absorption of photons in QWs is forbidden for certain combinations of initial and final states and polarization of the exciting field [27], we have calculated the complex dielectric function of QWs and incorporated it into our simulations to improve the accuracy of the modeled optical response of QWSCs, which is particularly important in the context of light trapping. In our approach, an initial calculation directly produces the absorption coefficient of a QW, α_{QW}, which is used to calculate the complex dielectric function using the relationship between α_{QW} and the extinction coefficient, and the appropriate Kramers-Kronig relations [28]. α_{QW} for an 8 nm $In_{0.3}Ga_{0.7}As/GaAs$ QW appears in Fig. 1, which illustrates the polarization dependence of absorption and which has peaks at wavelengths corresponding to resonant excitonic absorption in the QW sub-bands. The step-wise shape of $\alpha_{QW}(\lambda)$ at $\lambda > 850$ nm is based on the assumption that the QWs are true two-dimensional structures, which dictates the qualitative shape of their joint density of electronic states, $g(\hbar\omega)$, and, in turn, the shape of $\alpha_{QW}(\lambda)$ [26]. The complex dielectric function based on the data illustrated in Fig. 1 has been used in simulations involving 8 nm $In_{0.3}Ga_{0.7}As/GaAs$ QWs, and equivalent calculations have been performed to model QWs with different compositions that appear in this work.
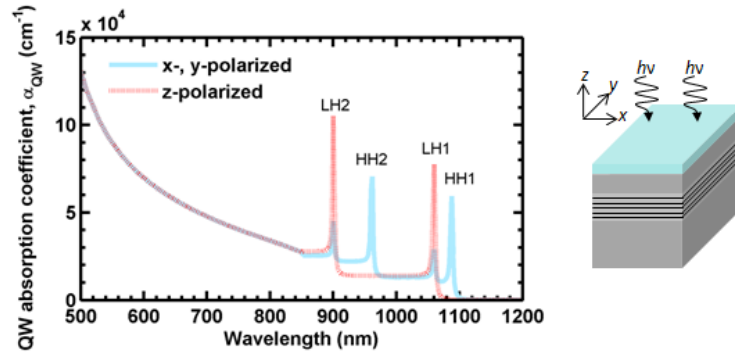

Fig. 1. The polarization-dependent absorption coefficient of an 8 nm $In_{0.3}Ga_{0.7}As/GaAs$ QW for ('x-, y-polarized') x- and y-polarized light and for ('z-polarized') z-polarized light, according to the coordinates shown in the illustration at right, at wavelengths corresponding to absorption in QW sub-band states ($\lambda > 850$ nm) and in the continuum of states ($\lambda \le 850$ nm). Peaks corresponding to resonant absorption by heavy-hole ('HH') and light hole ('LH') excitons are labeled, where the number in the exciton designation indicates the QW sub-band in which the exciton is generated. The absorption coefficient was calculated using the semi-empirical approach of Ref [26]. The calculated absorption coefficient spans the wavelength range 300 nm to 1200 nm, of which a subset is shown here to improve the clarity of features at $\lambda > 850$ nm.

Optical absorption and photocurrent generation in solar cells has been computed based on the net absorption of light by device structures in RCWA simulations. The RCWA solutions yield steady-state spatial distributions of electric and magnetic field amplitudes, and the normalized absorptivity in the semiconductor layers of a device at a given wavelength, $A_s(\lambda)$, assuming unity incident power. In this approach, $A_s(\lambda)$ is given by [29]:

$$A_s(\lambda) = \frac{\omega}{2}\int_{V_s}\varepsilon_2(\omega,\mathbf{r})\left|\mathbf{E}(\mathbf{r})\right|^2 d\mathbf{r}, \tag{1}$$

where ω is the angular frequency of the incident radiation, $\mathbf{r}$ is the position vector, $\varepsilon(\omega,\mathbf{r}) = \varepsilon_1(\omega,\mathbf{r}) + i\varepsilon_2(\omega,\mathbf{r})$ is the dielectric function, which varies according to the materials in the simulated volume of the device, and $\mathbf{E}(\mathbf{r})$ is the electric field vector. The integral in Eq. (1) is computed over the volume of semiconductor that comprises the active device, V_s, which is a subset of the total simulated device volume. In Fig. 2(a), which illustrates the prototypical

thin film QWSC structure with an integrated back side light trapping structure that we have simulated, the active device consists of the emitter, intrinsic, and base layers. In this work, device structures included metal in reflective and diffractive structures on the back of devices. Absorption in the metals is assumed not to contribute to the photocurrent of a device, which made it necessary to exclude that fraction of the total absorbed power from the photocurrent calculation. That has been achieved by specifying V_s in the simulation software such that photocurrent is calculated only from absorption in the active device layers.

Based on these quantities, the photocurrent density generated at a given wavelength, $j(\lambda)$, is a function of $A_s(\lambda)$, the incident photon flux at that wavelength, $\Phi_{ph}(\lambda)$, and the carrier collection efficiency, $\eta_C(\lambda)$, where it is assumed that each absorbed photon produces one electron-hole pair:

$$j(\lambda) = \Phi_{ph} \times A_S(\lambda) \times \eta_C(\lambda). \tag{2}$$

The short-circuit current density of a solar cell, J_{sc}, is then obtained by integrating over the full range of its spectral response:

$$J_{sc} = \int j(\lambda) d\lambda. \tag{3}$$

In general, light trapping structures for solar cells should be designed to maximize J_{sc}. If it is assumed that, for a given device structure, incorporating light trapping features does not affect V_{oc} or the fill factor of a device, then maximizing J_{sc} is equivalent to maximizing the efficiency. Quantifying the effect on V_{oc} and the fill factor of light trapping requires information about the electronic properties and carrier transport in the materials that comprise a device; such calculations are beyond the scope of this work.

Light trapping is achieved in this work via scattering of light by subwavelength-scale metal and dielectric diffractive structures on the back side of a solar cell. The process used here to optimize these structures for thin film QWSCs maximizes J_{sc} computed using Eqs. (1)-(3) for illumination under the AM 0 solar spectrum. In all simulations performed for this work, including those used in optimizations, light consisted of monochromatic plane waves incident normal to the device (i.e., in the -z direction based on the geometry of Fig. 2) with 45° linear polarization, which, in an average sense, accounts for the unpolarized nature of sunlight. Variable parameters of the light trapping structure, which was positioned immediately below the GaAs base layer of each device, are illustrated in Fig. 2(a). The thickness of an SiO$_2$ anti-reflection coating (ARC) on top of the device, denoted H$_1$ in Fig. 2(a), was also allowed to vary in optimizations in order to check the reasonableness of results. To do so, we assume that the proper ARC thickness maximizes J_{sc} by minimizing reflections at the wavelength corresponding to the absolute maximum of the incident photon flux, which is $\lambda \approx 600$ nm for the AM 0 spectrum. Using a single-layer SiO$_2$ ARC, that effect is achieved for H$_1 \approx 95$ nm; and all of the optimizations yielded H$_1 \approx 95$ nm, suggesting that each of the optimized light trapping structures was, in this sense, optimal, or nearly optimal.

The optimization began by using a genetic algorithm [30] to perform a broad search of the parameter space for planar, symmetric light trapping structures, which included periodic geometries that contained rectangular, triangular, hexagonal, spherical, or semi-spherical structures. The ranges of the parameters that were searched by the optimization were dictated by the measured photocurrent spectra of similar InGaAs/GaAs quantum well and quantum dot-in-well solar cells [31]. The parameters of light trapping structures produced by the genetic algorithm were then refined using a Simplex algorithm, which yielded the optimized diffractive structures that appear in this work. We note that the optimization was limited to relatively simple periodic structures similar to the rectangular one illustrated in Fig. 2(a), but which contained other geometric shapes previously mentioned. Rectangular structures similar to the one illustrated in Fig. 2(a) produced the highest J_{sc} of the various geometries that were optimized, and have therefore been used in this work. Structures with more complex

geometries may offer better light trapping performance if they are optimally engineered for coupling of light to optical modes of thin film devices.
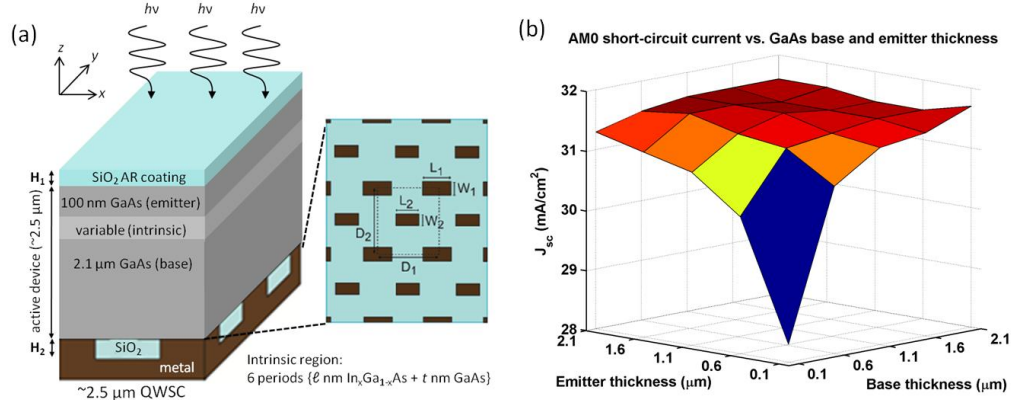

Fig. 2. (a) A representative diagram of the simulated device structures, which has a two-dimensional diffractive structure located on its back side with the following parameters defining it: the period in the x and y directions (D_1 and D_2, respectively); the pitch in those directions, which is collectively determined by W_1, W_2, L_1, and L_2; and the height of the grating, H_2. The device has an SiO_2 anti-reflection coating on the top surface, the thickness of which, H_1, is variable in optimizations. (b) J_{sc} of thin film QWSCs, computed as a function of the GaAs base and emitter thickness and assuming AM 0 illumination. The maximum J_{sc} over the range of simulated values of 31.7 mA/cm^2 is produced for a base thickness of 2.1 μm and an emitter thickness of 0.1 μm.

3. Analysis of thin film quantum well solar cells with diffractive structures

For this work, we simulated device structures corresponding to *p-i-n* diodes in which the GaAs emitter and base thickness, as well as the thickness of a nominally undoped intrinsic region, were initially variable, and later fixed for optimal performance. $In_xGa_{1-x}As$/GaAs QWs of variable composition (x), QW thickness, and barrier thickness have been simulated in order to quantify the effect of these parameters on J_{sc}. The back side geometry of the devices has also been varied to investigate effects associated with light trapping. This section discusses the influence of various electromagnetic phenomena on the response spectra of devices and how they influence J_{sc}.

3.1 Device thickness

While the most straightforward way to improve light absorption in a solar cell, in general, is to make it thicker, doing so often is not cost effective and may degrade V_{oc} or the fill factor of a device if it reduces η_C. In QWSCs, the thickness of the intrinsic region may be constrained by a minimum value for the built-in electric field that is required to collect carriers from sub-band states [21,22]. The base and the emitter layers offer more flexibility and principally require appropriate thicknesses to balance light absorption and carrier collection. J_{sc} of devices with variable total thickness, including an invariant intrinsic region composed of six periods of an {8 nm $In_{0.12}Ga_{0.88}As$/20 nm GaAs} QW, has therefore been calculated, assuming AM 0 illumination, to evaluate the relationship between device thickness and performance.

The results of J_{sc} *vs.* thickness calculations appear in Fig. 2(b), which shows that as the base and emitter thicknesses increase, J_{sc} converges rapidly to ~31.5 mA/cm^2 for a base thickness >0.6 μm. The changes in J_{sc} as a function of base and emitter thicknesses are asymmetric because of how they affect the position of the intrinsic region within the device structure. Ideally, the QWs spatially overlap with maxima in the electric field distribution, producing maximum absorption. These simulations used Pd in the rear reflector and

diffractive structure for consistency with other simulations and with fabricated devices. However, as the results in this work will demonstrate, Pd is sub-optimal for the reflective and diffractive structures because it strongly absorbs light, in particular at wavelengths $\lambda > 850$ nm, which are absorbed exclusively in QWs.

Figure 2(b) indicates that within the range of base and emitter thicknesses simulated, an optimal J_{sc} of 31.7 mA/cm^2 is achieved with a base thickness of 2.1 μm and an emitter thickness of 0.1 μm. Nominally, these thicknesses are compatible with efficient carrier collection because they are significantly less than 3 μm and 2 μm, which are, respectively, the minority electrons and hole diffusion lengths in GaAs [32–34] that is doped similarly to the base and emitter in efficient thin film GaAs solar cells [35,36]. In subsequent thin film QWSC simulations, therefore, a base thickness of 2.1 μm and an emitter thickness of 0.1 μm are used. This device geometry is referred to as the "~2.5 μm QWSC" in the remainder of this text, and Fig. 2(a) bears that label on account of its relevance to this work. Unless otherwise specified, the ~2.5 μm QWSC structure contains six periods of an {8 nm In$_{0.3}$Ga$_{0.7}$As/20 nm GaAs} QW in the intrinsic region, which is between the base and emitter; a 95 nm SiO$_2$ ARC on the top surface [i.e., H$_1$ = 95 nm, as indicated in Fig. 2(a)]; and the Pd-SiO$_2$ diffractive structure illustrated in Fig. 2(a).

3.2 Fabry-Perot interference

Fabry-Perot interference can significantly affect the response of a thin film solar cell due to the fact that a thin film will not, in general, absorb all low-energy photons, resulting in interference when the corresponding electromagnetic wave is reflected or scattered at the back surface of a device. Coupling of diffracted light to waveguide modes of a device structure occurs efficiently only when the momenta of scattered/diffracted waves match the momentum of a guided mode [37], which can be satisfied only by one wavelength for a given incident angle and period of a diffractive structure. In the diffractive structures investigated in this work, light that is not diffracted undergoes a combination of absorption in metallic features of the structure and specular reflection (zero order diffraction). The zero order diffracted fields interfere with the incident field, producing Fabry-Perot characteristics similar to those of a structure with a standard back reflector.

The effect of Fabry-Perot interference on the response of thin film QWSCs integrated with diffractive structures has been investigated by simulating the intermediate case of a planar, homogeneous film of SiO$_2$ of thickness H$_2$, inserted between the base layer of the device and the Pd reflector. Figure 3(a), 3(b) shows the simulated absorption response of devices with several back side geometries: planar, semi-infinite Pd immediately abutting the GaAs base layer of the device, which serves as a back side reflector and electrical contact (this geometry is referred to as 'Pd'); the same device, but with 165 nm of SiO$_2$ between the GaAs base layer and the semi-infinite Pd (referred to as 'SiO$_2$-Pd'); and the same device with an optimized back side diffractive structure having the geometry shown in Fig. 2(a) (referred to as 'SiO$_2$-Pd grating'). The spectral positions of features in the simulated absorption spectra of the 'SiO$_2$-Pd grating' device in Fig. 3(a) can be compared to the wavelengths at which resonant excitonic absorption occurs in the QWs, as seen in Fig. 1 and which are labeled in Fig. 3(a). Due to the relatively large strength of excitonic absorption, a light trapping structure may be particularly beneficial if it confines photons of energy resonant with that required for photogeneration of excitons to regions of a device where QWs are located.

As shown in Fig. 3(b), the 'Pd' device spectrum exhibits regular oscillations in absorptivity that are expected from Fabry-Perot interference for a planar reflector, and it has a peak absorption at $\lambda > 850$ nm (i.e., at wavelengths for which absorption in the active device occurs exclusively in QWs) of ~30%. The 'SiO$_2$-Pd' device spectrum also exhibits regular oscillations, though the positions of peaks and valleys in absorption are shifted in wavelength with respect to 'Pd' because of the phase shift in Fabry-Perot reflected waves associated with

the increased dielectric thickness from the SiO$_2$ interlayer. The peak absorption at $\lambda > 850$ nm also increases to ~45% with the inclusion of the dielectric interlayer, because light is reflected at the GaAs-SiO$_2$ interface, reducing loss due to absorption in the Pd.

Turning to the absorption spectrum of the device with an optimized Pd-SiO$_2$ diffractive structure ('SiO$_2$-Pd grating'), several features at $\lambda > 850$ nm are worth noting: (1) most of the peaks in absorption occur at the same wavelengths as for 'SiO$_2$-Pd'; (2) the exception to (1) is the peak at $\lambda = 1085$ nm, which coincides with the first heavy hole excitonic transition in the QW; (3) values of both the maxima and minima of absorption are larger for 'SiO$_2$-Pd grating' compared to 'SiO$_2$-Pd', by averages of ~5.0% and 5.5% in absolute absorptivity, respectively; (4) the widths of some of the absorption peaks have increased with respect to those in 'SiO$_2$-Pd' and 'Pd'. The net effect is evident in the simulated AM 0 J_{sc} for devices based on the absorption spectra in Fig. 3, which has been calculated according to Eqs. (2) and (3), assuming $\eta_C(\lambda) = 1$: 'Pd' corresponds to $J_{sc} = 32.9$ mA/cm^2; 'SiO$_2$-Pd' corresponds to $J_{sc} = 33.2$ mA/cm^2; and 'SiO$_2$-Pd grating' corresponds to $J_{sc} = 33.5$ mA/cm^2. In comparison, the reference GaAs homojunction structure produces $J_{sc} = 31.2$ mA/cm^2 with all three of the back side geometries investigated here. We note that the improvement achieved with a Pd-SiO$_2$ diffractive structure is considerably less than what may be achieved if the structure is realized using a metal that is less lossy than Pd, such as Ag, for which results appear in Fig. 3(d); the simulated AM 0 photocurrent corresponding to the 'SiO$_2$-Ag grating' spectrum [Fig. 3(d)] is $J_{sc} = 35.9$ mA/cm^2, which is 2.4 mA/cm^2 (~7%) greater than that of the 'SiO$_2$-Pd grating' device. The discussion here focuses on the Pd-SiO$_2$ structure because it corresponds to fabricated devices, for which measurement results may be found in Ref [26].

The simulation results show that J_{sc} improves by 0.3 mA/cm^2 from adding an SiO$_2$ interlayer between the GaAs base and Pd reflector/contact layers, which has no light trapping benefit, but which reduces loss due to absorption by Pd compared to the 'Pd' reflector/contact. That improvement equals approximately half of the 0.6 mA/cm^2 increase in J_{sc} achieved by the complete SiO$_2$-Pd diffractive structure, which, additionally, diffracts light into waveguide modes of the QWSC structure. Thus, the effects of absorption enhancement due to non-zero order diffraction, which can couple to waveguide modes, and of improving the response associated with zero order diffraction, equally benefit J_{sc} for the simulated devices.

The results in Fig. 3 also illustrate the effectiveness of light trapping in devices that contain strongly absorbing semiconductor structures, such as direct bandgap QWs. As illustrated in Fig. 1, the structure of α_{QW} implies that in the absence of a light trapping structure more light can be absorbed in the QW at $\lambda = 850$-950 nm than at $\lambda > 950$ nm, because α_{QW} is larger at the shorter wavelengths. Figure 3(d) demonstrates that is also true when the diffractive structures investigated in this work are integrated with the QWSCs, which is because optimization of the light trapping structures produced designs that are particularly effective for increasing broadband absorption in QWs to maximize J_{sc}. The net benefit for photocurrent generation of integrating these QWSCs with the diffractive structures investigated here is presented in Sec. 3.4.
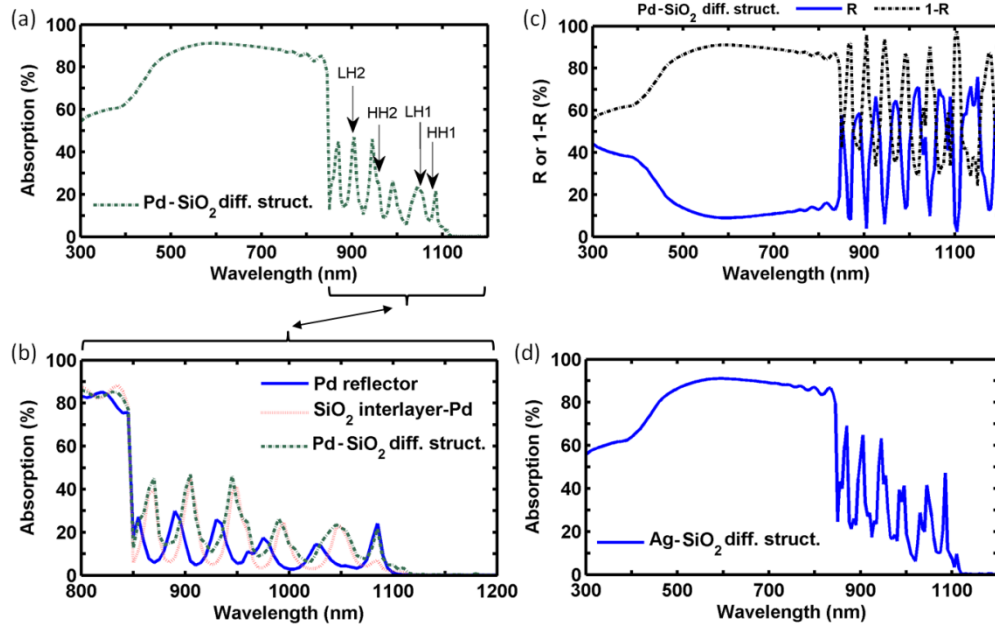
Fig. 3. Simulated optical response spectra for a ~2.5 μm QWSC, as illustrated in Fig. 2(a), with QWs composed of 8 nm $In_{0.3}Ga_{0.7}As$/20 nm GaAs, where the back side geometry consists of ('Pd reflector') semi-infinite Pd, ('SiO$_2$ interlayer-Pd') 165 nm SiO$_2$ followed by semi-infinite Pd, and ('Pd-SiO$_2$ diff. struct.') a Pd-SiO$_2$ diffractive structure or ('Ag-SiO$_2$ diff. struct.') a Ag-SiO$_2$ diffractive structure, which were optimized for this QWSC and which have the geometry shown in Fig. 2(a), where W_1 = 268 nm, L_1 = 800 nm, W_2 = 686 nm, L_2 = 205 nm, D_1 = 1355 nm, D_2 = 1070 nm, and H_2 = 165 nm. (a) illustrates the complete absorption spectrum of the 'Pd-SiO$_2$ diff. struct.' device and the wavelengths at which resonant absorption by heavy hole ('HH') and light hole ('LH') excitons occurs are marked. (b) illustrates the absorption spectra of QWSCs with each of the Pd-based back side geometries at wavelengths longer than the nominal GaAs absorption edge (850 nm). (c) illustrates the reflectivity ('R') and the net absorption ('1-R'), which includes loss due to metal absorption, when the Pd-SiO$_2$ diffractive structure was used. (d) illustrates the absorption spectrum of a QWSC with a diffractive structure made of Ag and SiO$_2$.

3.3 Spatial overlap of quantum wells and the electric field distribution

The refractive index of bulk $In_xGa_{1-x}As$, which was calculated by linear interpolation of the refractive index data for InAs [38] and GaAs [39], is close to that of GaAs for values of $x \leq$ 0.3 at the relevant solar wavelengths. Both refractive indices vary from ~3.5 to 4.5 at most of the relevant wavelengths, differing by an average of <10%, which implies that the multi-QW layers in the intrinsic region, which are surrounded by the GaAs base and emitter, constitute a relatively poor waveguide compared to, for example, Si-SiO$_2$ structures, for which the difference between their refractive indices is much larger [40].

The effective waveguide for a thin film InGaAs/GaAs QWSC is, therefore, the entire device structure rather than the multi-QW layers in the intrinsic region [41]. Thus, light is expected to couple to confined modes that occupy the entire device volume, rather than just the heterostructure layers. In that case, only a fraction of a waveguide mode will overlap with QWs in the intrinsic region of a device. For light that consists of photons with energy less than the bandgap of GaAs, only the portions of the associated fields that overlap with the QWs in the simulated device structures can be absorbed, including fields corresponding to light trapped in waveguide modes of such devices.

To demonstrate the effect of that spatial overlap on photocurrent generation, simulations of the ~2.5 μm QWSC device structure have been performed in which the multi-QW-

containing intrinsic region was located in a variety of positions within the device. As seen in Fig. 4(a), light at an incident wavelength of 860 nm couples to a high order waveguide mode with many nodes, while light at an incident wavelength of 1105 nm couples to a lower order mode with fewer nodes. Ideally, the region of a device that contains QWs would overlap with a maximum in field intensity between nodes. However, the intrinsic region is thin (~300 nm) compared to the total device thickness (~2.5 μm) and, therefore, QWs located in it are likely to overlap with a relatively small portion of a guided wave if the waveguide consists of the entire device structure, as in the InGaAs/GaAs QWSC structures studied here.
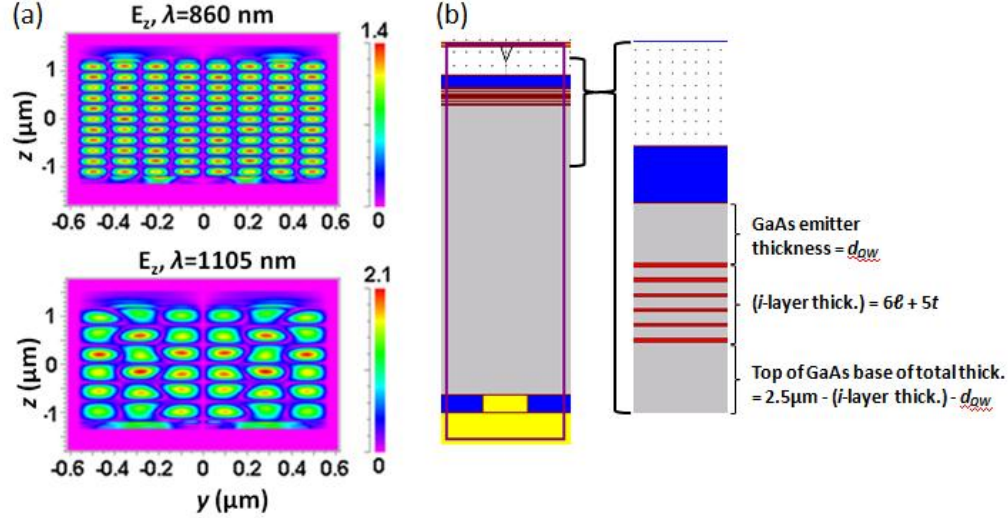
Fig. 4. (a) Cross-sectional plots at $x = 0$ [i.e., through the center of the unit cell of the diffractive structure shown in Fig. 2(a)] of the E_z component of the electric field in the ~2.5 μm QWSC structure, at incident wavelengths of 860 nm and (b) 1105 nm. The incident field is polarized in the x-y plane, so E_z corresponds to a component of the diffracted field, which is seen to couple to a high order waveguide mode for $\lambda = 860$ nm, and to a lower order mode for $\lambda = 1105$ nm. (b) An illustration of different device structures that were used in RCWA simulations to determine how J_{sc} of a QWSC with six periods of {λ nm In$_{0.3}$Ga$_{0.7}$As / t nm GaAs} varies according to the position of QWs in the device, d_{QW}, where λ is the thickness of the QW and t is the thickness of the QW barrier. The total thickness of the device is the same for each simulated structure (~2.5 μm). All of the illustrations in this figure correspond to $\lambda = 8$ nm and $t = 20$ nm. The device is integrated with an optimized Pd-SiO$_2$ diffractive structure similar to the one illustrated in Fig. 2(a).

The effect of the overlap of the multi-QW-containing intrinsic region of the device with the electric field distribution in the device structure was investigated for the ~2.5 μm QWSC by adjusting the InGaAs QW thickness, λ, the thickness of the GaAs barriers between the QWs, t, and the depth of the intrinsic region from the top of the active device structure, d_{QW}, while keeping the total device thickness constant. Figure 4(b) illustrates how the device structure changes as a function of those parameters. The modes supported by the device are minimally affected by these variations because the refractive index of the waveguide is essentially unchanged, due to the similar refractive indices of InGaAs and GaAs. Thus, coupling of light into modes of the device structure is essentially invariant with QW thickness, barrier thickness, and the position of the intrinsic region for the simulated InGaAs/GaAs structures.

The simulated AM 0 J_{sc} of a ~2.5 μm thick InGaAs/GaAs QWSC is plotted as a function of d_{QW} in Fig. 5. Simulations used values for λ of 5 nm, 10 nm, and 20 nm, and values for t of 20 nm and 40 nm. While realistic values of λ and t for solar cells depend on numerous

considerations, such as the desired absorption spectrum and the critical thickness of the heterostructure, the values used in this work were chosen because they represent a range of generally reasonable QW and barrier thicknesses based on the critical thicknesses for InGaAs/GaAs heterostructures [42,43].

As seen in Fig. 5, for a given value of λ, J_{sc} can vary by up to ~2 mA/cm^2 solely as a consequence of positioning of the QWs that achieves better or worse overlap with the field intensity profile in the device structure. The intensity profile includes normally incident and reflected waves, and waves that propagate in waveguide modes following coupling to them via diffraction or scattering. Figure 5(b), 5(d) indicates that the largest J_{sc} generally occurs for $d_{QW} = 25$ nm regardless of whether $t = 20$ nm or $t = 40$ nm, indicating a benefit of locating the intrinsic region, which contains the QWs, near the top of the device. This relates to the electric field distribution in the ~2.5 μm QWSC structure, which contains a minimum in the mode profile (i.e., a node) that generally occurs at the top of the semiconductor region. Thus, in the device structure, the volume of semiconductor within ~200 nm of the top of the semiconductor never contains a local minimum in the optical mode for the wavelengths of interest, and locating the intrinsic region there, which contains strongly absorbing QWs, yields a photocurrent maximum.
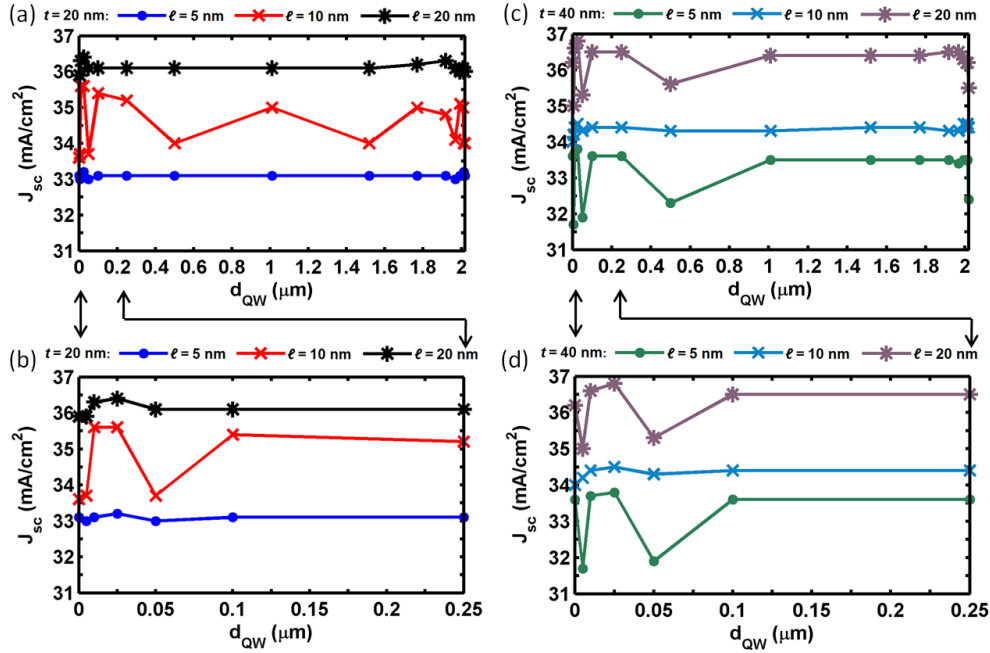

Fig. 5. Variation of the AM 0 J_{sc} of devices with optimized back side diffractive structures as a function of the thickness of the depth of the multi-QW structure from the GaAs emitter, d_{QW}, for selected values of the InGaAs QW thickness, λ, and the GaAs barrier thickness, t, as illustrated in Fig. 4(b). (a,c) illustrate the full range of d_{QW} that was simulated for $t = 20$ nm and $t = 40$ nm, respectively, while (b,d) focus on device structures where the multi-QW layer is located near the top of the active layers, also for $t = 20$ nm and $t = 40$ nm, respectively.

The average value of J_{sc} increases as λ increases because the absorption coefficient of the QWs is higher than the absorption coefficient of GaAs at most of the relevant wavelengths. Thus, if carriers photogenerated in QW sub-band states are collected efficiently regardless of the QW thickness, it is advantageous to use thick QWs for InGaAs/GaAs devices because they absorb a greater fraction of incident power than thin QWs for a given number of QWs and a given QW composition.

Certain combinations of λ and t produce J_{sc} that exhibits obvious minima and maxima as d_{QW} varies, while other combinations produce almost negligible variation of J_{sc} with d_{QW}. The data show that the variation cannot be predicted simply from the value of λ or of t: certain combinations result in negligible J_{sc} vs. d_{QW} variation while others result in significant J_{sc} vs. d_{QW} variation, as seen in Fig. 5. Furthermore, there is not one value of λ or of t that determines the magnitude of variation of J_{sc} vs. d_{QW}, and many more combinations of each parameter exist than were feasible for simulation. Thus, it should be assumed that the performance of any thin film QWSC with a device structure and light trapping structure that are similar to those simulated here is sensitive to the QW thickness (λ), the barrier thickness (t), and the position of the QWs within the device. The results in Fig. 5 demonstrate that J_{sc} for such devices can vary by more than 5% depending on the values of those parameters, corresponding to 1-2 mA/cm^2 of photocurrent under AM 0 illumination in the simulated device structures. The variation of J_{sc} with such parameters is a direct result of the position of the QWs with respect to the spatial distribution of light intensity in the device, which may be determined by a combination of reflection, transmission, diffraction, scattering, and absorption.

3.4 Photocurrent enhancement trends in thin film quantum well solar cells

In order to evaluate the overall improvement of photocurrent that may be expected in QWSCs utilizing the light trapping structures investigated in this work, the AM 0 J_{sc} of ~2.5 μm thick device structures with six periods of {8 nm In$_x$Ga$_{1-x}$As/20 nm GaAs} in the intrinsic region, integrated with the optimized diffractive structures illustrated in Fig. 2(a), is compared to the same device structures with planar metal reflectors/contacts. The relationship between J_{sc} and the atomic fraction of indium, x, of the In$_x$Ga$_{1-x}$As QWs is plotted in Fig. 6(a), and is summarized in Table 1, for cases where either Ag or Pd are used as the planar reflector/contact or as the metal in the diffractive structure. The case of $x = 0$ corresponds to a GaAs homojunction device.
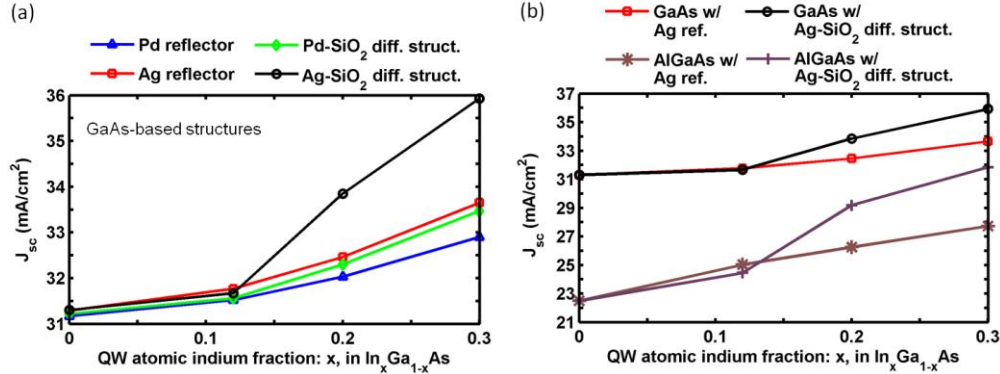

Fig. 6. The simulated AM 0 J_{sc} as a function of QW composition (x in In$_x$Ga$_{1-x}$As) for ~2.5 μm thick QWSCs, for $x = 0.12$, 0.20, and 0.30. (a) InGaAs/GaAs QWSCs were simulated with different back side geometries: a planar Pd reflector/contact ('Pd reflector'); a planar Ag reflector/contact ('Ag reflector'); and optimized diffractive structures that consist of Pd and SiO$_2$ ('Pd-SiO$_2$ diff. struct.') or Ag and SiO$_2$ ('Ag-SiO$_2$ diff. struct.'). (b) The data designated by the prefix "GaAs w/" is the same as that shown in (a) for the specified back side geometries. The data designated by the prefix "AlGaAs w/" corresponds to simulations of device structures equivalent to the "GaAs w/" devices, but where all GaAs in the device was replaced by Al$_{0.29}$Ga$_{0.71}$As. Devices were simulated with two of the same back side geometries as in (a): a planar Ag reflector/contact ('Ag reflector') or with optimized diffractive structures that consist of Ag and SiO$_2$ ('Ag-SiO$_2$ diff. struct.').

Several important conclusions can be drawn from the data in Fig. 6(a) and Table 1:

(1) Inserting relatively few InGaAs/GaAs QWs (<10 periods) into the intrinsic region of a thin film *p-i-n* GaAs homojunction device can produce substantial increases in photocurrent, which are significantly larger when the diffractive structures investigated in this work are used instead of planar back side reflectors/contacts. That results from increased absorption in the semiconductor layers due to diffracting light into modes, including waveguide modes, increasing the path length of photons; and from reduced parasitic metal absorption in the diffractive structures relative to planar reflectors. Compared to GaAs homojunction devices, the AM 0 J_{sc} of ~2.5 μm thick $In_xGa_{1-x}As$/GaAs QWSCs increases by up to 4.6 mA/cm^2 (15%) for QW compositions $x \leq 0.3$ when devices are integrated with a diffractive structure made of Ag and SiO$_2$. The greatest improvement occurs for the most strongly absorbing QWs that were simulated (In$_{0.3}$Ga$_{0.7}$As).

(2) The metal used to implement the diffractive structures can significantly influence their light trapping efficacy. If Ag is used in the diffractive structure instead of Pd, $J_{sc}(x)$ improves considerably for QWSCs in which QWs with $x > 0.15$ are used, due to reduced absorption in Ag compared to Pd. Reduced absorption in the metal features of the diffractive structures enables more light to be diffracted at all orders. The net benefit of using Ag-SiO$_2$ diffractive structures is an increase in the AM 0 J_{sc} of ~2.5 μm thick QWSCs with $In_xGa_{1-x}As$/GaAs QWs for $x > 0.2$ of at least 1 mA/cm^2 compared to devices with Ag reflectors/contacts.

(3) $J_{sc}(x)$ benefits most from light trapping when diffractive structures are used with $In_xGa_{1-x}As$/GaAs QWs that have large atomic fractions of indium, because the absorption coefficient of $In_xGa_{1-x}As$ increases, and its bandgap decreases, with x.

Table 1. AM 0 J_{sc} (mA/cm^2) of InGaAs/GaAs devices[a]

Rear geometry	GaAs homojunction	In$_{0.12}$Ga$_{0.88}$As	In$_{0.2}$Ga$_{0.8}$As	In$_{0.3}$Ga$_{0.7}$As
Pd reflector	31.2	31.5	32.0	32.9
Pd-SiO$_2$ diff. struct.	31.2	31.6	32.3	33.5
Ag reflector	31.3	31.8	32.5	33.7
Ag-SiO$_2$ diff. struct.	31.3	31.7	33.9	35.9

[a]The table summarizes the data of Fig. 6(a) and has row labels identical to the labels in the legend of that figure, which identify the back side geometry of devices. The QW compositions are indicated by the column labels, including a reference device with no QWs ('GaAs homojunction').

The result that $J_{sc}(x)$ increases in proportion to the absorption coefficient of $In_xGa_{1-x}As$ suggests that significant averaging of Fabry-Perot and diffraction effects occurs over the absorption bandwidth of the QWs, so that, ultimately, the greatest benefit is realized when QWs with relatively large atomic fractions of indium (or, potentially quantum dots or other strongly absorbing semiconductor structures) are used. The averaging likely relates to the narrow range of wavelengths at which diffractive structures can strongly couple incident light to waveguide modes of a device structure, which is a fundamental aspect of their periodicity. Nevertheless, diffractive structures with multiple periods, such as those used here, can outperform single-period diffractive structures (i.e., linear gratings) [44], and additional optimization of their geometry, and of device structures, should yield further improvement.

While this work has focused on InGaAs/GaAs QWSCs, the light trapping structures in this work can significantly improve the performance of other thin film III-V QWSCs. Using the intermediate value of $x = 0.2$ from the range of $In_xGa_{1-x}As$ QW compositions investigated in this work, which has a nominal bandgap of ~1.06 eV [45], detailed balance calculations indicate that the optimal barrier material for a QWSC has a bandgap of ~1.77 eV, based on the results of Ref [14]. Using $Al_xGa_{1-x}As$ as a barrier, a bandgap of ~1.77 eV is achieved with Al$_{0.29}$Ga$_{0.71}$As based on data in Refs. [45] and [46]. GaAs$_y$P$_{1-y}$ could also be used as the barrier material, for which GaAs$_{0.58}$P$_{0.42}$ achieves a bandgap of ~1.77 eV, based on data in Ref [45]. A likely advantage of replacing GaAs with AlGaAs or GaAsP in the simulated QWSC structures is that a device made from either of the larger bandgap materials would have a higher nominal V_{oc} than equivalent GaAs-based QWSCs. The improved voltage coincides

with reduced J_{sc} because fewer photons are absorbed by the larger bandgap materials, but the power conversion efficiency could be significantly higher.

To investigate the influence of light trapping structures on an optimal QWSC structure based on $In_{0.2}Ga_{0.8}As$ QWs, simulations analogous to those used to produce the data illustrated in Fig. 6(a) have been performed, but in which the GaAs base, emitter, and QW barriers in the device structure illustrated in Fig. 2(a) were replaced by ~1.77 eV bandgap $Al_{0.29}Ga_{0.71}As$. We substituted $Al_{0.29}Ga_{0.71}As$ for GaAs because it is nearly lattice-matched to GaAs, so the physical structure of the AlGaAs-based QWSC, and notably strain in the device, can be expected to be comparable to the GaAs-based QWSCs in this work, which is important for consistency of the modeled QW absorption data used in the simulations.

Figure 6(b) shows the estimated AM 0 J_{sc} for a simulated $InGaAs/Al_{0.29}Ga_{0.71}As$ QWSC with an Ag back reflector and for the equivalent device structure with the same optimized Ag-SiO_2 diffractive structure used for InGaAs/GaAs QWSCs in Fig. 2(a). Table 2 summarizes the data of Fig. 6(b), and, for comparison, they both also contain data from Table 1 and Fig. 6(a), respectively, for the simulated InGaAs/GaAs QWSC. As expected, J_{sc} for the $InGaAs/Al_{0.29}Ga_{0.71}As$ QWSCs are significantly less than those of the corresponding InGaAs/GaAs QWSCs because $Al_{0.29}Ga_{0.71}As$ absorbs many fewer photons than GaAs when the thickness of the materials is the same, as in these simulations. However, the relative improvement of J_{sc} that results from replacing a planar Ag reflector with the diffractive structure is considerably higher for the $InGaAs/Al_{0.29}Ga_{0.71}As$ QWSCs (~15%) than for InGaAs/GaAs QWSCs (~7%) because, for broadband solar power harvesting, the InGaAs QWs are much closer to optimal for wide bandgap $Al_{0.29}Ga_{0.71}As$ than for GaAs. Therefore, with respect to the potential advantage of generating higher voltages than would be expected from InGaAs/GaAs QWSCs by implementing devices based on wide-bandgap materials, such as $Al_{0.29}Ga_{0.71}As$ or $GaAs_{0.58}P_{0.42}$; and, in consideration of the effectiveness of back side diffractive structures for improving photocurrent generation in III-V thin film solar cells that contain InGaAs QWs: these results suggest that optimization of thin film QWSCs with integrated light trapping structures is generally applicable to tailoring the performance of high efficiency thin film solar cells to suit the electrical requirements of a solar power system.

Table 2. AM 0 J_{sc} (mA/cm^2) of InGaAs/AlGaAs and InGaAs/GaAs devices[b]

Rear geometry	Homojunction	$In_{0.12}Ga_{0.88}As$	$In_{0.2}Ga_{0.8}As$	$In_{0.3}Ga_{0.7}As$
GaAs w/ Ag reflector	31.3	31.8	32.5	33.7
GaAs w/ Ag-SiO$_2$ diff. struct.	31.3	31.7	33.9	35.9
AlGaAs w/ Ag reflector	22.5	25.0	26.3	27.7
AlGaAs w/ Ag-SiO$_2$ diff. struct.	22.5	24.5	29.2	31.9

[b]The table summarizes the data of Fig. 6(b) and has row labels identical to the labels in the legend of that figure, which identify device materials and the back side geometry of devices. The QW compositions are indicated by the column labels, including reference devices with no QWs ('Homojunction').

Finally, Fig. 6 and Tables 1-2 illustrate that light trapping can be of great benefit when it is utilized with strongly absorbing materials, such as direct bandgap QWs. Various works have calculated the *relative* improvement of absorption in a semiconductor in the weakly absorbing limit, which can reach very high values $\geq 4n^2$, where n is the refractive index of the semiconductor [44,47,48]. However, the *absolute* change in J_{sc} as a result of absorption enhancement in the weakly absorbing limit may still be small due to the fact that the weakly absorbing limit assumes the electromagnetic field intensity in the semiconductor absorber is essentially constant, implying negligible absorption of light. As this work demonstrates, light trapping can significantly improve J_{sc} of thin film devices by targeting absorption in strongly absorbing active layers. This is a compelling approach to realizing high efficiency solar cells in versatile thin film geometries, and one which may be generally useful for optimizing photocurrent generation in device structures that require absorption of low energy photons in a limited volume of semiconductor, such as intermediate band solar cells [9,49].

7. Summary

In summary, light absorption in thin film InGaAs/GaAs quantum well solar cells benefits from the use of planar, multi-periodic back side diffractive structures, which diffract light into waveguide modes of the device structures, and which minimize loss associated with planar metal reflectors/back contacts. The shape of the response spectra of such devices are significantly influenced by the Fabry-Perot characteristics of the thin device film. For the range of diffractive structures studied, they improved the simulated AM 0 J_{sc} of ~2.5 μm thick $In_xGa_{1-x}As$/GaAs QWSCs by up to 2.2 mA/cm^2 (7%) relative to the same devices with planar metal reflectors, and by up to 4.6 mA/cm^2 (15%) compared to ~2.5 μm thick GaAs homojunction devices, for QWs with $x \leq 0.3$. For InGaAs/$Al_{0.29}Ga_{0.71}As$ structures with more optimal combinations of QW and barrier bandgaps for QWSCs, J_{sc} improvements of up to ~42% relative to an $Al_{0.29}Ga_{0.71}As$ homojunction device with a planar Ag reflector appear to be attainable. The improvements resulted equally from coupling of diffracted waves into waveguide modes of the device structures and from reduced parasitic absorption in the diffractive structures compared to planar metal reflectors. Irrespective of using a diffractive structure or a planar reflector, the greatest benefit for J_{sc} is realized by using $In_xGa_{1-x}As$ QWs with relatively large atomic fractions of indium (x), assuming that photogenerated carriers are collected from the QWs, due to the fact that the QW absorption coefficient increases, and its absorption edge increases to longer wavelengths, with x. It may also be important to consider the position of QWs within such devices because these parameters can affect the short-circuit current density by more than 5%, potentially corresponding to several mA/cm^2 of photocurrent. The results presented here support an approach to realizing high-efficiency solar cells based on semiconductor heterostructures, including but not limited to QWSCs, that utilizes light trapping to realize high levels of photocurrent generation and power conversion efficiency for a broad range of spectral illumination conditions.

Acknowledgments